Proceedings of DETC'98
1998 ASME Design Engineering Technical Conferences
September 13-16, 1998, Atlanta, Georgia

DETC98/DAC-5605

NOVEL EMPIRICAL SIMILARITY METHOD FOR THE RELIABLE PRODUCT TEST WITH RAPID PROTOTYPES

Uichung Cho, Kristin L. Wood, and Richard, H. Crawford
Manufacturing and Design Research Laboratory
Department of Mechanical Engineering
The University of Texas at Austin
Austin, Texas 78712-1063
Email:uichung@mail.utexas.edu

ABSTRACT

Contemporary industries are devoting increasing attention to the product development process, due to tight market shares and the abridged product life cycle. Reliable scaled product testing with rapid prototypes has the potential to improve these processes by replacing traditional costly and time-consuming product tests. In this context, rapid prototypes provide visual, ergonomic, and functional information with minimal time delay. Among the information classes, reliable functional information is least realized because of several features of rapid prototypes: (1) limited material choices and part size; (2) distinct material structure; (3) restrictive loading conditions; and (4) state-dependent material properties. To develop reliable functional tests, an improved similarity method is needed to overcome these limitations. The traditional similarity method, based on a Buckingham Π approach, is commonly applied to perform scaled tests. In contrast to this method, wherein the state transformation between two similar systems is derived from dimensional vectors, we present a new similarity method that empirically derives the transformation from a geometrically simple specimen pair. The primary advantage of the new method over the traditional method is the capability to relate highly distorted systems. In this paper, the concept and theoretical framework of the novel similarity method are introduced, and two numerical examples demonstrate the new method.

Keywords: Product development, Buckingham Π theorem, Similarity Method, Rapid Prototyping, Scaled functional testing, Distorted similarity, Empirical state transformation

1 INTRODUCTION

The objective of a similarity method is to experimentally predict the behavior of a target system through an indirect scaled testing, alleviating complex system construction and testing effort. Traditionally, a scaled physical model that can show similar behavior is designed on the basis of the Buckingham Π theorem, and the behavior of the target system is estimated from the mathematically derived scaling laws (Kline, 1965; Baker et al., 1991). In some special cases, more expensive scaled-up models are prepared (Burton et al., 1967). However, it is typical to geometrically scale down (Mixson and Catherine, 1964), to change materials (Wright and Bannister, 1971), and/or to simplify models (Fay, 1993) in order to reduce the physical modeling effort. In the context of product design, an improved similarity method, aided by advanced prototyping techniques, may accelerate design processes if it can yield reliable predictions with relaxed restrictions on scaled models.

Product design is a recursive and iterative process that relies on various kinds of information to transform customer needs into concepts, embodied and detailed virtual products, and finally physical products. Industries utilize both virtual and physical models to procure reliable information. Even though the applicable problem domains and accuracy of virtual models are increasing, the industrial trend is to verify and adjust product performance and quality through physical testing. Based on this practice, Wall et al. investigated and evaluated several prototyping techniques (Stereolithography, rubber molding, CNC machining) (Wall et al., 1991). According to their study, rapid prototyping usually requires the least cost and time for the fabrication of a single part, but rapid prototyping materials are too limited to perform diverse functional tests.

Rapid prototyping or solid freeform fabrication is a relatively new set of technologies that can effectively fabricate

geometrically complex parts directly from CAD data without part specific tooling. Since the late 1980's, several unique rapid prototyping techniques have been developed and advanced. Most of the systems can fabricate geometrically complex prototypes within approximately 50 hours, where polymers are the most popular base material (Aubin, 1994). In some industries, rapid prototypes are already being used to enhance communication, to detect design faults early, and to build patterns or molds for casting (Jacobs, 1992). Some functional tests are also performed with rapid prototypes thanks to improved geometric accuracy and strength, but these tests are limited to certain problem domains.

Surprisingly, very little literature exists on the functional testing with rapid prototypes (Dornfeld, 1995; Steinchen et al., 1995). Most such studies are based on traditional similarity, and are limited to experimentally examining the test results without providing a way to improve test results. In the traditional similarity method, the corresponding dimensionless parameters of the rapid prototype and the product should be kept identical. However, this condition cannot always be satisfied due to the limited prototyping materials and size, uncertain system parameters, and restricted loading conditions. Additionally, the method presumes similarity of material behavior (e.g., stress-strain curve) and structure (e.g., isotropic) between two systems. These presumptions may be violated as (1) material behavior varies from one material to another; and (2) material structure is dependent on fabrication processes.

To overcome such problems, this paper introduces a new empirically based similarity method. The concept of the new similarity method is motivated from two observations: (1) the information utilized by the traditional method (dimensional vectors) is too restrictive; and (2) the cost and time for physical modeling is highly dependent on geometrical complexity. Instead of dimensional vectors, a correlation between two geometrically complex systems is empirically derived from geometrically simple specimens. The details of the concept and applications are presented in the following section.

2 LIMITATIONS IN SCALED TESTING WITH RAPID PROTOTYPES

To clarify the necessity of a new similarity method, the traditional similarity method is briefly introduced. In addition, the current status of rapid prototyping techniques is described.

2.1 Traditional Similarity Method

The two main applications of the Buckingham Π theorem are:

- To provide a means of significantly reducing the effort to build empirical models by reducing the number of required experiments (dimensional analysis).
- To design a scaled system, and to predict the behavior of the system of interest by testing this scaled system. This application is known as similarity, the similitude method, or comparative dimensional analysis (emphasizing two systems).

The first approach is inappropriate for our purposes, as it focuses on effective modeling through the real system, not a scaled one. The fundamentals of the Buckingham Π theorem will be mathematically described by highlighting comparative dimensional analysis.

2.1.1 Mathematical Framework of the Π theorem

In general, the functional relationship between a state of interest X and n independent system parameters P_i can be represented as follows:

$$X = f(P_1, P_2, \cdots, P_n) \tag{1}$$

where the function f is unknown. If X and the P_i involve k fundamental dimensions (e.g., mass, length, time, temperature), $(d_1, d_2, \cdots, d_k)$, then the dimension of X and each P_i can be represented as

$$[X] = \prod_{j=1}^{k} d_j^{R_j(X)}$$
$$[P_i] = \prod_{j=1}^{k} d_j^{R_j(P_i)} \tag{2}$$

where the exponents, $R_j(X)$ and $R_j(P_i)$, are rational numbers which are dependent on X and P_i respectively.

The dimension vector α is defined as a $k \times 1$ column vector composed of exponents of the fundamental dimensions:

$$\alpha(P_i) = \left[R_1(P_i) \;\; R_2(P_i) \;\; \cdots \;\; R_k(P_i)\right]^T. \tag{3}$$

Taking dimension vectors as column vectors, the dimension matrix **B** of n system parameters is defined as the $k \times n$ matrix,

$$\mathbf{B} = \left[\alpha(P_1) \;\; \alpha(P_2) \;\; \cdots \;\; \alpha(P_n)\right]. \tag{4}$$

If the rank of **B** is ρ, the system can be represented with $N = n - \rho$ dimensionless parameters. The N dimensionless parameters can be derived from the linearly independent N general solutions $\mathbf{x}_p^i$ of

$$\mathbf{B} \cdot \mathbf{x}_p = \mathbf{0}. \tag{5}$$

If $\mathbf{x}_p^i = \left(\omega_1^i \;\; \omega_2^i \;\; \cdots \;\; \omega_n^i\right)^T$, then the N dimensionless parameters can be expressed as

$$\pi_i = \prod_{j=1}^{n} P_j^{\omega_j^i} \tag{6}$$

where i=1, 2, … , N.

Similarly, the dimensionless parameter that includes state variable X can be represented as $\pi_X = X \cdot \prod_{i=1}^{n} P_i^{\xi_i}$, where the ξ_i's are solutions of $\mathbf{B} \cdot \left(\xi_1 \;\; \xi_2 \;\; \cdots \;\; \xi_n\right)^T = -\alpha(X)$.

With the derived π_X and π_i's, the system represented by Eq. (1) can be equivalently expressed as

$$\pi_X = F(\pi_1, \pi_2, \cdots, \pi_N). \tag{7}$$

Barr introduced the echelon matrix procedure as a systematic method to derive dimensionless parameters with several interesting examples (Barr, 1984).

2.1.2 Comparative Dimensional Analysis

Consider two systems $\sum_A$ and $\sum_B$, that can be represented as

$$X^A = f(P_1^A, P_2^A, \cdots, P_n^A), \quad X^B = f(P_1^B, P_2^B, \cdots, P_n^B) \tag{8}$$

where the P_i's are system parameters that are related to system geometry, material and loading conditions. These systems can also be equivalently represented as

$$\pi_X{}^A = F(\pi_1{}^A, \pi_2{}^A, \cdots, \pi_N{}^A), \quad \pi_X{}^B = F(\pi_1{}^B, \pi_2{}^B, \cdots, \pi_N{}^B) \tag{9}$$

where π_i's are dimensionless parameters, which are related to the P_i's.

If $\pi_i{}^A = \pi_i{}^B$ for any i=1, 2, … , N, then $\pi_X{}^A = \pi_X{}^B$ from Eq. (9). As a result, one can predict X^A from the following *prediction equation*

$$X^A = X^B \cdot \frac{\prod_{i=1}^{n} (P_i^B)^{\xi_i}}{\prod_{i=1}^{n} (P_i^A)^{\xi_i}} \tag{10}$$

if all system parameters of $\sum_A$ do not violate any of the *similarity constraints*,

$$\prod_{j=1}^{n} (P_j^A)^{\omega_j^i} = \prod_{j=1}^{n} (P_j^B)^{\omega_j^i}, \tag{11}$$

for all i=1, 2, …, N. When all of these constraints are satisfied, two systems are defined as *well-scaled*; otherwise, *distorted* or *badly-scaled*.

For convenience and consistency, deriving scaling laws from Eqs. (10) and (11) is preferred. The scaling laws are compact representations of Eqs. (10) and (11), and they are functions of scale factors (Baker et al. 91). The scale factor of a system parameter P is defined as $\lambda_p = \frac{P_t}{P_p}$. Here the subscript t and p denote *the target system* whose states are to be predicted, and *the prototype* which is prepared for scaled testing.

The traditional similarity method derives the prediction equation and similarity constraints (Eqs. (10) and (11)) assuming that the two system equations can be represented in the same functional form, as shown in Eq. (8). However, this assumption may not be valid due to following reasons:

- limited material choices and dimensions of available scaled models;
- unknown boundary conditions; and
- difficulties in realizing desired boundary conditions.

The new similarity method aims to eliminate or mitigate these problems by testing a specimen pair thus generating more information about the system. In the new method, n corresponding states of $\sum_A$ and $\sum_B$ are related by a $n \times n$ matrix, instead of the prediction Eq. (11), and the similarity constraints in Eq. (11) need not to be satisfied, as the identity of the functional form of two systems is not postulated.

2.2 Rapid Prototyping Techniques

Rapid prototyping offers an approach to getting physical models much more quickly than through conventional means. However, it becomes more difficult to construct well-scaled systems when one utilizes rapid prototypes as scaled models, mainly due to material issues.

2.2.1 Commercial Systems

Commercial rapid prototyping systems can fabricate geometrically complex parts, but they impose restrictions on part size and material choices. As the similarity constraints, Eq. (11), are coupled functions of system parameters (related to part size, material, and loading conditions), construction of well-scaled rapid prototypes is not always possible. To understand these limitations, Tables 1 and 2 summarize part size and available materials in current commercial rapid prototyping systems. Larger size capacities and ranges of material properties are currently being developed in the industry.

2.2.2 Advances in Rapid Prototyping Techniques

The fabrication of electrical interconnects and *in situ* sensors (Beck et al., 1992; Sun et al., 1997; Safari et al., 1997) is a noticeable research area for functional testing with rapid prototypes. Rapid prototypes with electrical interconnects and *in situ* sensors open new avenues for functional testing by enhancing the monitoring of the internal system behavior. The effort to embed sensors (Halwel and Klameckl, 1991), and the application of embedded sensors (Smith et al., 1992) to smart structures, shows the possibility and necessity of these techniques.

Table 1. Price Comparison of Rapid Prototyping Systems

Company	System	Capacity L^3 (mm^3)	Cost C (1,000 $)	C/L^3
3D Systems	SLA-250/30	250x250x250	215	0.86
	SLA-500/20	584x508x508	495	0.97
	SLA-500/30	584x508x508	540	1.06
EOS GmbH	STEROS300	300x300x250	290	0.97
	STEROS400	400x400x300	380	0.95
	STEROS600	600x600x400	500	0.83
D-MEC	JSC 2000	500x500x500	500	1.0
	JSC 3000	1000x800x500	750	0.9
Cubital	Solider 4600	350x350x350	325	0.9
	Solider 5600	500x350x500	550	1.0

Table 2. Materials available for Rapid Prototyping

Company	Base Materials
3D Systems Inc.	Liquid Photopolymer (Epoxy resin)
Helisys Inc.	Paper coated with Polyethylene
Soligen Inc.	Ceramic powder with liquid binder
Statasys Inc.	Investment casting wax, Polyolefin, Polyamide
DTM	Nylon, Polycarbonate, ProtoFrom composite, TruForm PM, Polymer coated sand and bronze etc.
Laser 3D	Photopolymer
C-MET	Hard polymer, Rubber
D-MET Ltd.	Urethan acrylate

Recently, efforts to fabricate prototypes with multiple and functionally gradient materials (Griffith et al., 1997; Jepson et al., 1997; Fessler et al., 1997) are emerging as a new research area. Rapid prototyping with functionally gradient materials may enable the fabrication of prototypes with manufacturing process dependent characteristics (e.g., surface hardening of parts after annealing). Such advancements will aid in the ability to create prototypes with desired material properties.

Along with these relatively new studies, research to fabricate geometrically accurate parts with desired functional attributes (e.g, strength, water resistance, heat resistance) has been continuously carried out. Owing to this effort, opportunities to utilize rapid prototypes as functional prototypes have dramatically increased. However, functional tests with rapid prototypes may produce erroneous test results mainly due to following reasons:

- Most rapid prototyping processes, such as Stereolithography, Selective Laser Sintering, Shape Deposition, and 3D printing, fabricate parts by continuously generating contoured layers from a sheet, liquid, or powder, and combining the layers (Aubin, 1994). Due to the layer-additive or subtractive fabrication schemes, most rapid prototypes show orthotropic material structure in some degree (Nelson et al., 1993). In extreme cases, rapid prototypes show delamination of layers.
- In spite of significant effort to expand the types of base materials, polymers are still the most popular and dependable materials. Polymers show distinct material behavior from that of metals (Birley et al., 1988).

3 NOVEL EMPIRICAL SIMILARITY METHOD FOR DISTORTED SIMILARITY PROBLEMS

Several Π theorem based studies have been carried out for distorted similarity problems (Murphy, 1971; Bazant, 1994; Farrar et al., 1994). Among them, Murphy proposed a strategy to relax the similarity constraints by casting the prediction equation into a more complex form. He converted a simple linear prediction equation to a nonlinear equation, and demonstrated how to derive the corresponding design constraints inversely through a forced vibration example. Aided by his method, one can design prototype systems with different restrictions on system parameters when the system equation is known.

Table 3. Comparison of Traditional and New Empirical Similarity Method

	Traditional Method	New Empirical Method
Theoretical Basis	Π theorem	Symmetry Method, BEM
Required Conditions	• Identity of configuration of governing equations and corresponding π terms • Constant system parameters • Geometrical similarity	Geometrical similarity between the prototype and the product.
Prediction Equation for *n* states	$X_{Mi} = \lambda_X \cdot X_{Pi}$ where I=1,2,…,n	$\begin{Bmatrix} X_1^{\,t} \\ \vdots \\ X_n^{\,t} \end{Bmatrix} = \mathbf{T} \cdot \begin{Bmatrix} X_1^{\,p} \\ \vdots \\ X_n^{\,p} \end{Bmatrix}$
Applicable Domain	Theoretically no limitation	Boundary value problems

In parallel to the dimensional analysis based studies, the symmetry method can be utilized to solve similarity problems. The symmetry method, originated by Sophus Lie, aims to find solutions to hard-to-solve nonlinear differential equations from those of similar linear differential equations. For boundary value problems, the symmetry method can be considered as a generalization of dimensional analysis (Bluman and Kumei, 1989). However, one needs to know the governing equations in the form of partial differential equations beforehand.

Most existing studies attempt to solve specific distorted similarity problems on the basis of mathematical models and/or results obtained through extensive experiments. In contrast, we derive a state transformation through single specimen testing without knowledge of the governing equations and material properties. As the name implies, the new method empirically derives the relationship between the corresponding states of a prototype and its governing product from a specimen pair. The new method concentrates on relating corresponding solutions of two distinct boundary value problems, as we are interested in problems with complex boundary contours. In comparison to the traditional similarity method, which is based on the Buckingham Π theorem, our new method relaxes restrictions on the prototype and loading conditions – potentially requiring only geometrical similarity. Table 3 summarizes these distinctions.

3.1 Similarity Transformation Matrix

The prediction Eq. (11) can be represented as

$$X^A = X^B \cdot \prod_{i=1}^{n} \left(\frac{P_i^B}{P_i^A} \right)^{\xi_i} = X^B \cdot \lambda_X . \tag{12}$$

The scale factor λ_X becomes constant once the prototype system parameters are chosen such that none of the constraints on the prototype is violated. In general continuum problems, the relationship between states of Σ_A and Σ_B at $n \cdot m$ corresponding temporal and spatial points p_i and p_i^* can be expressed as

$$\begin{bmatrix} X^A(p_1) & X^A(p_{n+1}) & \cdots & X^A(p_{n(m-1)+1}) \\ X^A(p_2) & X^A(p_{n+2}) & \cdots & X^A(p_{n(m-1)+2}) \\ \vdots & \vdots & \ddots & \vdots \\ X^A(p_n) & X^A(p_{2n}) & \cdots & X^A(p_{nm}) \end{bmatrix}$$

$$= \begin{bmatrix} \lambda_X \cdot X^B(p_1^*) & \lambda_X \cdot X^B(p_{n+1}^*) & \cdots & \lambda_X \cdot X^B(p_{n(m+1)+1}^*) \\ \lambda_X \cdot X^B(p_2^*) & \lambda_X \cdot X^B(p_{n+2}^*) & \cdots & \lambda_X \cdot X^B(p_{n(m-1)+2}^*) \\ \vdots & \vdots & \ddots & \vdots \\ \lambda_X \cdot X^B(p_2^*) & \lambda_X \cdot X^B(p_{2n}^*) & \cdots & \lambda_X \cdot X^B(p_{nm}^*) \end{bmatrix}$$

$$= \lambda_X \cdot \mathbf{I} \cdot \begin{bmatrix} X^B(p_1^*) & X^B(p_{n+1}^*) & \cdots & X^B(p_{n(m+1)+1}^*) \\ X^B(p_2^*) & X^B(p_{n+2}^*) & \cdots & X^B(p_{n(m-1)+2}^*) \\ \vdots & \vdots & \ddots & \vdots \\ X^B(p_2^*) & X^B(p_{2n}^*) & \cdots & X^B(p_{nm}^*) \end{bmatrix} \tag{13}$$

if $m \geq n$. If not, the state transformation matrix is not unique. At first glance, Eq. (13) seems to be trivial. However, this equation is fundamental to the empirical similarity method, and the following theorem can be deduced from this equation.

> **Theorem 1**. *State Transformation matrix for well-scaled systems*
>
> The matrix that relates *any* corresponding $n \times 1$ state vectors of two well-scaled systems should be diagonal and its diagonal terms should be identical (scaled identity matrix).

3.2 Concept of the new similarity method

Let Σ_T be a target system, whose sub-state vector $\mathbf{X}_T$ is of interest. When Σ_T requires considerable fabrication effort due to its geometrical complexity, it is desirable to predict $\mathbf{X}_T$ from the corresponding state vector $\mathbf{X}_P$ of a geometrically similar prototype Σ_P. As we attempt to dramatically reduce the prototyping effort, Σ_P may be fabricated from a rapid prototyping process. It is postulated that a reliable relationship between $\mathbf{X}_T$ and $\mathbf{X}_P$ cannot be derived from the traditional similarity method as the two systems may be distorted due to their distinct fabrication characteristics.

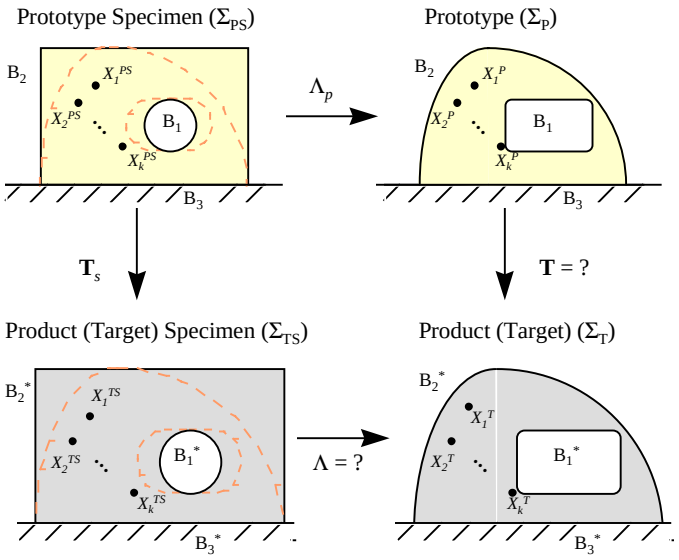

Figure 1. State Transformation between Prototype, Target, and Specimen Pairs

In comparison to the traditional similarity method that utilizes dimension vectors, the new method derives a relationship between $\mathbf{X}_P$ and $\mathbf{X}_T$ from a specimen pair, as shown in Figure 1. One specimen system Σ_{TS} is constructed with the same fabrication process as Σ_T (e.g., traditional machining), and the other system Σ_{PS} with that of Σ_P (e.g., SLS process). Boundary conditions on Σ_{TS} and Σ_{PS} are imposed similar to Σ_T and Σ_P, respectively, as shown.

As a preliminary approach, a linear transformation matrix $\mathbf{T}$ that satisfies the following equation,

$$\mathbf{X}_{TS} = \mathbf{T} \cdot \mathbf{X}_{PS} \tag{14}$$

is derived from a specimen pair, so that $\mathbf{X}_T$ can be predicted from

$$\mathbf{X}_T = \mathbf{T} \cdot \mathbf{X}_P . \tag{15}$$

In order to make the transformation matrix $\mathbf{T}$ consistent, the remaining problems in realizing this new concept are:

- How to determine $\mathbf{T}$ from Eq. (14), as the $\mathbf{T}$ that satisfies Eq. (14) is not unique;
- How to design the specimen pair and impose boundary conditions; and
- How to choose measurement points on the specimen pair,

3.3 Determination of the Transformation Matrix

The derivation of the transformation matrix T that satisfies Eq. (14) is an undetermined problem, as the state vectors are n by 1, where n is the number of measurement points, and T is an n by n matrix. So, we need constraints or an objective function to find a meaningful transformation matrix.

From Theorem 1, we postulate:

Proposition 1.1: *Transformation for distorted systems*

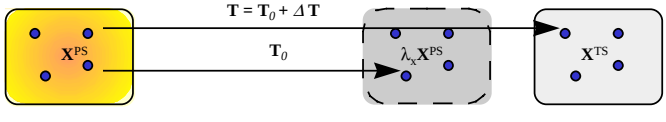

Figure 2. The state transformation between two distorted systems

If there exists a consistent linear state transformation between two distorted systems, the transformation can be expressed as the combination of a dominant scaled identity matrix and a compensation matrix that reflects the pure system distortion.

Based on this statement, it is assumed that the diagonal norm of the similarity transformation matrix for distorted systems is maximal, where the diagonal norm of a $n \times n$ matrix $\mathbf{T}$ is defined as

$$\|\mathbf{T}\|_D = \sum_{i=1}^{n} t_{ii}^{\,2} \tag{16}$$

where $j=1,2,\ldots,n$. t_{ij} is an element of $\mathbf{T}$. In order to maximize $\|\mathbf{T}\|_D$, $\mathbf{T}$ is derived by perturbing the initial matrix $\mathbf{T}_0$ defined as

$$\mathbf{T}_0 = \mu(\lambda_X) \cdot \mathbf{I}_n . \tag{17}$$

$\mathbf{I}_n$ is the $n \times n$ identity matrix and the mean scale factor $\mu(\lambda_X)$ is defined as

$$\mu(\lambda_X) = \frac{1}{n} \cdot \sum_{i=1}^{n} \frac{X_{TS}(p_i)}{X_{PS}(p_i^*)} \tag{18}$$

where the subscripts *TS* and *PS* denote the target and prototype specimens.

The complete state transformation $\mathbf{T}$ is

$$\mathbf{T} = \mathbf{T}_0 + \delta\mathbf{T}, \tag{19}$$

where $\delta\mathbf{T}$ needs to be found. As shown in Figure 2, the initial similarity transformation matrix $\mathbf{T}_0$ can be considered the state transformation, considering that the prototype system is well-scaled, and $\delta\mathbf{T}$ can be considered the compensation matrix that represents the purely distorted state transformation.

From Eqs. (14) and (19),

$$\mathbf{X}_{TS} = (\mathbf{T}_0 + \delta\mathbf{T}) \cdot \mathbf{X}_{PS}, \tag{20}$$

and a particular solution $\delta\mathbf{T}$ that minimizes its maximum singular value can be approximated from

$$\delta\mathbf{T} = (\mathbf{X}_{TS} - \mathbf{T}_0 \cdot \mathbf{X}_{PS}) \cdot \mathbf{X}_{PS}^{\,+}. \tag{21}$$

Here, $\mathbf{X}_{ps}^{\,+}$ is the Moore-Penrose pseudo-inverse matrix that satisfies

$$\begin{aligned} \mathbf{X}_{ps} \cdot \mathbf{X}_{ps}^{\,+} \cdot \mathbf{X}_{ps} &= \mathbf{X}_{ps} \\ \mathbf{X}_{ps}^{\,+} \cdot \mathbf{X}_{ps} \cdot \mathbf{X}_{ps}^{\,+} &= \mathbf{X}_{ps}^{\,+}. \end{aligned} \tag{22}$$

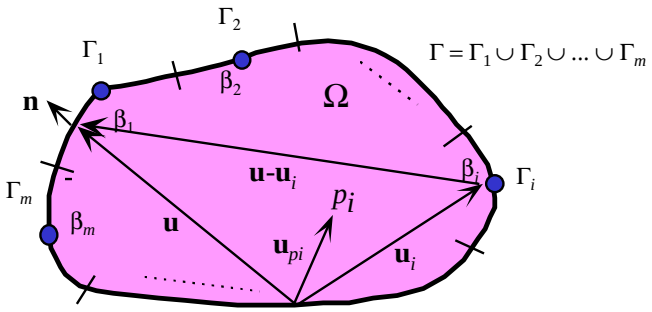

β_i: nodal point, Γ_i: boundary element, Ω: interior domain, Γ: boundary surface

Figure 3. Boundary Element Representation of a 2D Problem

If $\delta\mathbf{T}$ is negligible, the two systems can be considered well-scaled. The matrix norm of $\delta\mathbf{T}$ can be considered a measure for estimating the degree of distortion between the two systems.

3.4 Partial Proof of the New Similarity Method

The boundary element method, a relatively new numerical method that solves various boundary value problems (Gipson, 1987; El-Zafrany, 1993; Ingham, 1994), has the potential to mathematically prove (or disapprove) the validity of the new similarity method. In comparison to the finite element or finite difference method that constructs a system matrix as a coupled relation between states at all nodal points, the boundary element method constructs a system matrix that relates only the states of interest. Due to this unique feature, the boundary element method can be used as a vehicle with which one can investigate the relationship between states at arbitrary finite points of the prototype and the target.

3.4.1 Boundary Element Representation of 2D Problems

Consider a simple 2D problem as shown in Figure 3. The solid object of interest can be represented by the two dimensional domain Ω and the boundary surface Γ, and either natural (e.g., heat flux, traction) or forced boundary conditions (e.g., temperature, displacement) should be known at all boundary nodal points. It should be noted that a forced boundary condition should be given at least at one nodal point.

The boundary element method converts differential equations and boundary conditions into a boundary integral equation, and discretizes the equation into matrix form. At first, the complete boundary condition pairs (forced and natural) at all nodal points β_{ij} are derived by utilizing the given boundary conditions, Green's function of a given problem, and the boundary shape from

$$\mathbf{H} \cdot \Phi = \mathbf{G} \cdot \mathbf{Q}\,^{1}. \tag{23}$$

[1] In general, there can be an additional term to represent concentrated source (Poisson's term). However, the term is not considered here for simplicity.

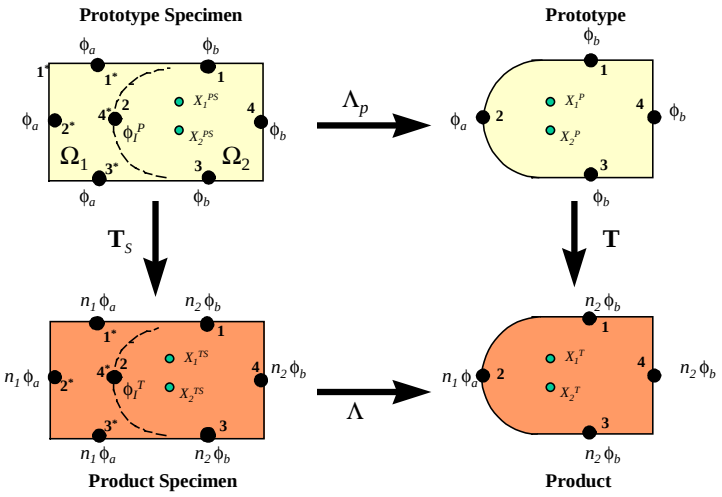

Figure 4. Simplified Boundary Value Problem

$\Phi = \begin{pmatrix}\phi_1 & \phi_2 & \cdots & \phi_m\end{pmatrix}^T$ and $\mathbf{Q} = \begin{pmatrix}q_1 & q_2 & \cdots & q_m\end{pmatrix}^T$ denote forced and natural boundary conditions respectively, where the subscript is the node number. At every node, either a natural or a forced boundary condition should be given. Here, the $m \times m$ matrices **H** and **G** can be determined from the Green's function and the boundary shape (Gipson, 1987).

When mixed boundary conditions are given, one should rearrange Eq. (23) by swapping columns of **H** and **G**, and rows of Φ and **Q,** in order to make all unknowns appear on one side. From the rearranged equation, one can find the unknown ϕ_i's and q_i's. Once the complete Φ and **Q** are derived, the state $X(p_i)$ at any point p_i in Ω can be derived from

$$\begin{pmatrix}X(p_1) & X(p_2) & \cdots & X(p_k)\end{pmatrix}^T = \mathbf{h}\cdot\Phi + \mathbf{g}\cdot\mathbf{Q} \qquad (24)$$

where **h** and **g** are $k \times m$ matrices.

3.4.2 Proof of the New Method

With the boundary element method, states of four simple boundary value problems shown in Figure 4 are derived in order to investigate the state transformation between the four systems. It is assumed that only forced boundary conditions are given to avoid swapping of elements. **T** is the similarity transformation that abstracts the state change due to the variation of non-geometric parameters. In comparison, the geometric transformation Λ represents the state change due to the variation of the geometry, with the other system parameters remaining constant.

By considering region 1, Ω_1, of the prototype specimen, the natural boundary condition can be derived from Eq. (23),

$$\begin{Bmatrix}q_{1'}\\ q_{2'}\\ q_{3'}\\ q_{4'}\end{Bmatrix} = \begin{bmatrix}\mathbf{r}_1^{\,p1}\\ \mathbf{r}_2^{\,p1}\\ \mathbf{r}_3^{\,p1}\\ \mathbf{r}_4^{\,p1}\end{bmatrix}\cdot\begin{Bmatrix}\phi_a\\ \phi_a\\ \phi_a\\ \phi_I^{\,p}\end{Bmatrix} \qquad (25)$$

where $\mathbf{r}_i^{\,p1}$ is a 1×4 row vector of $\mathbf{G}^{-1}\cdot\mathbf{H}$ for Ω_1 of the prototype specimen. Similarly, the natural boundary condition of Ω_2 becomes

$$\begin{Bmatrix}q_1\\ q_2\\ q_3\\ q_4\end{Bmatrix} = \begin{bmatrix}\mathbf{r}_1^{\,p2}\\ \mathbf{r}_2^{\,p2}\\ \mathbf{r}_3^{\,p2}\\ \mathbf{r}_4^{\,p2}\end{bmatrix}\cdot\begin{Bmatrix}\phi_b\\ \phi_I^{\,p}\\ \phi_b\\ \phi_b\end{Bmatrix} \qquad (26)$$

where $\mathbf{r}_i^{\,p2}$ is a 1×4 row vector of $\mathbf{G}^{-1}\cdot\mathbf{H}$ for Ω_2 of the prototype specimen..

By applying the compatibility condition, $q_{4'} = -q_2$

$$\begin{aligned}&\mathbf{r}_4^{\,p1}\cdot\begin{pmatrix}\phi_a & \phi_a & \phi_a & \phi_I^{\,p}\end{pmatrix}^T\\ &= -\mathbf{r}_2^{\,p2}\cdot\begin{pmatrix}\phi_b & \phi_I^{\,p} & \phi_b & \phi_b\end{pmatrix}^T\end{aligned} \qquad (27)$$

and $\phi_I^{\,p} = C(r_{44}^{\,p1} + r_{22}^{\,p1})\cdot\left[\phi_a\cdot f_a(\mathbf{r}_4^{\,p1}) + \phi_b\cdot f_b(\mathbf{r}_2^{\,p2})\right]$. The details of the functions C, f_a and f_b are shown in Appendix 1. From Eqs. (24) and (27), $\mathbf{X}_{ps}$, the 2×1 state vector of Ω_2 of the prototype specimen, can be expressed as

$$\begin{aligned}\mathbf{X}_{ps} &= \begin{bmatrix}\mathbf{h}_1^{\,p}\\ \mathbf{h}_2^{\,p}\end{bmatrix}\cdot\begin{Bmatrix}\phi_b\\ \phi_I^{\,p}\\ \phi_b\\ \phi_b\end{Bmatrix} + \begin{bmatrix}\mathbf{g}_1^{\,p}\\ \mathbf{g}_2^{\,p}\end{bmatrix}\cdot\begin{Bmatrix}q_1\\ q_2\\ q_3\\ q_4\end{Bmatrix}\\ &= \begin{bmatrix}\mathbf{h}_1^{\,p}\\ \mathbf{h}_2^{\,p}\end{bmatrix}\cdot\begin{Bmatrix}\phi_b\\ \phi_I^{\,p}\\ \phi_b\\ \phi_b\end{Bmatrix} + \begin{bmatrix}\mathbf{g}_1^{\,p}\\ \mathbf{g}_2^{\,p}\end{bmatrix}\cdot\begin{bmatrix}\mathbf{r}_1^{\,p2}\\ \mathbf{r}_2^{\,p2}\\ \mathbf{r}_3^{\,p2}\\ \mathbf{r}_4^{\,p2}\end{bmatrix}\cdot\begin{Bmatrix}\phi_b\\ \phi_I^{\,p}\\ \phi_b\\ \phi_b\end{Bmatrix}\\ &= \left(\begin{bmatrix}\mathbf{h}_1^{\,p}\\ \mathbf{h}_2^{\,p}\end{bmatrix} + \begin{bmatrix}\mathbf{g}_1^{\,p}\\ \mathbf{g}_2^{\,p}\end{bmatrix}\cdot\begin{bmatrix}\mathbf{r}_1^{\,p2}\\ \mathbf{r}_2^{\,p2}\\ \mathbf{r}_3^{\,p2}\\ \mathbf{r}_4^{\,p2}\end{bmatrix}\right)\cdot\begin{Bmatrix}\phi_b\\ U_1\\ \phi_b\\ \phi_b\end{Bmatrix}\\ &= \mathbf{A}_p\cdot\begin{pmatrix}\phi_b & U_1 & \phi_b & \phi_b\end{pmatrix}^T,\end{aligned} \qquad (28)$$

where $U_1 = C(\mathbf{r}_4^{\,p1}, \mathbf{r}_2^{\,p2})\times[\phi_a\cdot f_a(\mathbf{r}_4^{\,p1}) + \phi_b\cdot f_b(\mathbf{r}_2^{\,p2})]$.

Eq. (28) can be reorganized as

$$\mathbf{X}_{ps} = \mathbf{A}_p \cdot \mathbf{Q}_p \cdot \Phi_p$$

where,

$$\mathbf{Q}_p = \begin{bmatrix} 1 & 0 & 0 & 0 \\ C(\mathbf{r}_4^{p1}, \mathbf{r}_2^{p2}) & C(\mathbf{r}_4^{p1}, \mathbf{r}_2^{p2}) & 0 & 0 \\ \times f_b(\mathbf{r}_2^{p2}) & \times f_a(\mathbf{r}_4^{p1}) & & \\ 0 & 0 & 1 & 0 \\ 0 & 0 & 0 & 1 \end{bmatrix} \tag{29}$$

$$\Phi_p = \begin{pmatrix} \phi_b & \phi_a & \phi_b & \phi_b \end{pmatrix}^T$$

and $\mathbf{Q}_p$ is not unique.

Applying the same approach to the prototype, the state vector of the prototype becomes

$$\mathbf{X}_p = \mathbf{A}_p \cdot \Phi_p, \tag{30}$$

as only the boundary conditions of Ω_2 of the prototype specimen and the prototype are distinct.

In the same manner, the state vectors of the target specimen and the target can be expressed as

$$\mathbf{X}_{ts} = \left(\begin{bmatrix} \mathbf{h}_1^t \\ \mathbf{h}_2^t \end{bmatrix} + \begin{bmatrix} \mathbf{g}_1^t \\ \mathbf{g}_2^t \end{bmatrix} \cdot \begin{bmatrix} \mathbf{r}_1^{t2} \\ \mathbf{r}_2^{t2} \\ \mathbf{r}_3^{t2} \\ \mathbf{r}_4^{t2} \end{bmatrix} \right) \cdot \begin{Bmatrix} n_2 \cdot \phi_b \\ U_2 \\ n_2 \cdot \phi_b \\ n_2 \cdot \phi_b \end{Bmatrix}$$

$$= \mathbf{A}_t \cdot \begin{bmatrix} 1 & 0 & 0 & 0 \\ C(\mathbf{r}_2^{t2}, \mathbf{r}_4^{t1}) & C(\mathbf{r}_2^{t2}, \mathbf{r}_4^{t1}) & 0 & 0 \\ \times f_b(\mathbf{r}_2^{t2}) & \times f_a(\mathbf{r}_4^{t1}) & & \\ 0 & 0 & 1 & 0 \\ 0 & 0 & 0 & 1 \end{bmatrix} \cdot \begin{Bmatrix} n_2 \cdot \phi_b \\ n_1 \cdot \phi_a \\ n_2 \cdot \phi_b \\ n_2 \cdot \phi_b \end{Bmatrix}$$

$$= \mathbf{A}_t \cdot \mathbf{Q}_t \cdot \Phi_t \tag{31}$$

where $U_2 = C(\mathbf{r}_2^{t2}, \mathbf{r}_4^{t1}) \times [n_1 \cdot \phi_a \cdot f_a(\mathbf{r}_4^{t1}) + n_2 \cdot \phi_b \cdot f_b(\mathbf{r}_2^{t2})]$

and

$$\mathbf{X}_t = \mathbf{A}_t \cdot \Phi_t. \tag{32}$$

On the basis of the derived Eqs. (29),(30),(31) and (32), the similarity and geometric state transformations for the following typical cases can be examined. In order to reduce the complexity of the problem, a specific case will be considered, and the other cases will be examined through numerical simulations. As a specific case, the situation when two systems are distorted purely due to boundary conditions is considered.

If there exists a certain ideal boundary condition that results in a scaled identity similarity transformation matrix, then two systems are defined to be distorted solely due to boundary conditions. The ideal boundary condition, which makes two systems well-scaled, cannot be applied to the prototype when exact boundary conditions are not known or not realizable.

Let the ideal boundary condition for prototypes be defined as $\Phi_{pi} = \mathbf{N} \cdot \Phi_t$, where $\mathbf{N}$ is a diagonal matrix whose elements become identical if either purely natural or purely free boundary conditions are applied. From Theorem 1, the similarity transformation should be a scaled identity matrix, $\lambda\mathbf{I}$, with this ideal loading condition, and

$$\begin{aligned} \mathbf{X}_{ts} - \lambda\mathbf{I} \cdot \mathbf{X}_{ps} &= \mathbf{A}_t \cdot \mathbf{Q}_t \cdot \Phi_t - \lambda \cdot \mathbf{A}_p \cdot \mathbf{Q}_p \cdot \Phi_{pi} \\ &= \mathbf{W}_t \cdot \mathbf{A}_t \cdot \Phi_t - \lambda \cdot \mathbf{W}_p \cdot \mathbf{A}_p \cdot \mathbf{N} \cdot \Phi_t \\ &= 0 \end{aligned} \tag{33}$$

from Eqs. (29) and (31), where

$\mathbf{W}_p = \mathbf{A}_p \cdot \mathbf{Q}_p \cdot \mathbf{A}_p^{-1}$ and $\mathbf{W}_t = \mathbf{A}_t \cdot \mathbf{Q}_t \cdot \mathbf{A}_t^{-1}$.

From Eq. (33),

$$\mathbf{N} = \frac{1}{\lambda} \mathbf{A}_p^{-1} \cdot \mathbf{W}_p^{-1} \cdot \mathbf{W}_t \cdot \mathbf{A}_t \tag{34}$$

as Eq. (33) should hold for any non-zero Φ_t. By substituting Eq. (34) into Eqs. (30) and (32),

$$\begin{aligned} \mathbf{X}_t - \lambda\mathbf{I} \cdot \mathbf{X}_p &= \mathbf{A}_t \cdot \Phi_t - \lambda \cdot \mathbf{A}_p \cdot \Phi_{pi} \\ &= \mathbf{A}_t \cdot \Phi_t - \frac{\lambda}{\lambda} \mathbf{A}_p \cdot \mathbf{A}_p^{-1} \cdot \mathbf{W}_p^{-1} \cdot \mathbf{W}_t \cdot \mathbf{A}_t \cdot \Phi_t \\ &= (\mathbf{A}_t - \mathbf{W}_p^{-1} \cdot \mathbf{W}_t \cdot \mathbf{A}_t) \cdot \Phi_t \\ &= 0, \end{aligned} \tag{35}$$

as the similarity transformation should be identical even when the system geometry is changed. From Eq. (35), the condition for distortion due to pure boundary conditions becomes

$$\mathbf{W}_p = \mathbf{W}_t. \tag{36}$$

This condition makes the geometric transformation of the target pair and the prototype pair equivalent, as

$$\begin{aligned} \Lambda &= \mathbf{W}_p \cdot \mathbf{A}_p \cdot \Phi_p \\ &= \mathbf{W}_p \cdot \mathbf{X}_p, \end{aligned} \tag{37}$$

and

$$\begin{aligned} \Lambda_t &= \mathbf{W}_t \cdot \mathbf{A}_t \cdot \Phi_t \\ &= \mathbf{W}_t \cdot \mathbf{X}_t, \end{aligned} \tag{38}$$

even when the boundary conditions are distorted.

To check the consistency of the similarity transformation, assume that there exists a consistent transformation $\mathbf{T}$ that simultaneously satisfies

$$\begin{aligned} \mathbf{X}_{ts} &= \mathbf{W}_t \cdot \mathbf{A}_t \cdot \Phi_t \\ &= \mathbf{T} \cdot \mathbf{W}_p \cdot \mathbf{A}_p \cdot \Phi_p = \mathbf{T} \cdot \mathbf{X}_{ps}, \end{aligned} \tag{39}$$

and

$$\begin{aligned} \mathbf{X}_t &= \mathbf{A}_t \cdot \Phi_t \\ &= \mathbf{T} \cdot \mathbf{A}_p \cdot \Phi_p = \mathbf{T} \cdot \mathbf{X}_p. \end{aligned} \tag{40}$$

By substituting (40) into (39), the following restriction that keeps the similarity transformation consistent can be derived:

$$\mathbf{W} \cdot \mathbf{T} - \mathbf{W} \cdot \mathbf{T} = 0 \tag{41}$$

where $\mathbf{W} = \mathbf{W}_t = \mathbf{W}_p$. If the matrix $\mathbf{T}$ is a scaled identity matrix, the RHS of (41) becomes zero; if not, it deviates from zero. So, $\|\mathbf{T}\|_D$ is maximized to make the similarity transformation $\mathbf{T}$ as precise as possible. This results in a partial proof of Proposition 1.1 for a specific case – when two systems are distorted due to boundary conditions only.

In summary, the approximate similarity transformation between the target and the prototype can be derived from a specimen pair. If the derived transformation $\mathbf{T}_s$ is not a scaled identity matrix, it may be distinct from the target transformation, $\mathbf{T}$. A method to refine the transformation(See subsection 3.3) is necessary. In contrast, the geometric transformation Λ for the target and the prototype is identical to Λ_s for the specimen pair, if:

- the two systems are distorted due to boundary conditions only; and
- the same boundary condition can be imposed on the prototype specimen and the prototype, and on the specimen pair.

4 NUMERICAL EXAMPLES

As a complement to the partial proof of the new similarity method, numerical simulations are performed with ANSYS™ in order to validate the concept of the new empirical similarity method.

4.1 Slotted Rod

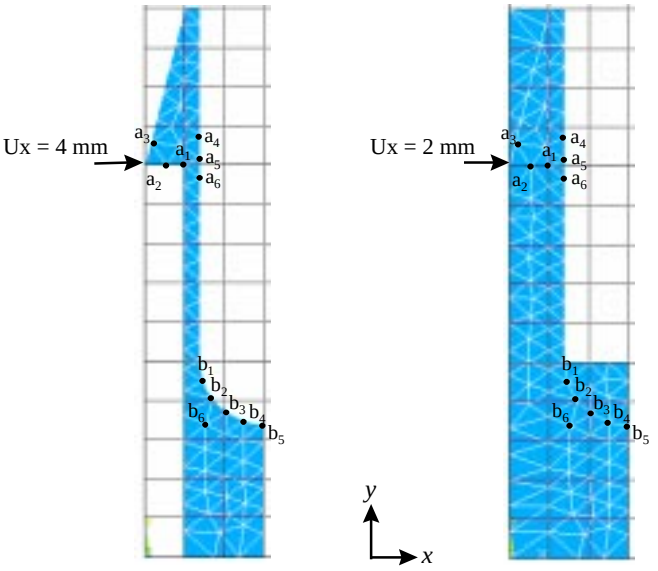

(a) Slotted Rod (b) Specimen Rod

(Thickness t=5mm, Grid size: 5 × 5 mm)

Figure 5. FE Model of symmetric half of the Nylon and Aluminum Slotted Rod, and the Specimen Pair

Virtual models for static structural problems are fairly well established. However, modeling of nonlinear structures, from the determination of stress with large deformation to the variation of stiffness after repeated loads, still requires advancements in virtual modeling (Fertis, 1993). A simple slotted rod example is introduced to demonstrate the capability of the new similarity method to correlate the stress of isotropic and orthotropic structures with large deformation.

Table 4. Material Property and Simulation Options for the Rod Example

Young's Modulus (GN/m^2)	• Aluminum: E_x= E_y=69 • Nylon: E_x=15, E_y=10
Poisson's Ratio	0.3
ANSYS Simulation Options	• Large deformation • Accuracy level = 3 • Linear stress-strain curve (Fully elastic) • Auto meshing (Level 4)

The stress of an aluminum slotted rod (Figure 5a) at the potential failure point set $A=\{a_1,a_2,\ldots,a_6\}$ is predicted using ANSYS™ to simulate the stresses of the specimen pair (Figure 5b) and nylon slotted rod, where the nylon rods are assumed to be fabricated from a rapid prototyping process. In order to test the influence of the location of the measurement point on the specimen pair, another point set $B=\{b_1,b_2,\ldots,b_6\}$ is also considered. Considering that the maximum stress level is encountered when the front end just passes through a hole, the x-directional displacement Ux is given as 4mm assuming the radius of the hole is 11mm (see Figure 5a). In the case of the specimen pair, half of Ux (2mm) is applied in order to keep the behavior similar to that of the slotted rod by maintaining the stress level below the proportional limit.

We assume that the Young's modulus of aluminum is isotropic whereas that of the rapid prototyping material is orthotropic[2]. In this situation, the reliable prediction of product stresses from that of the prototype is difficult with the traditional similarity method as discussed in Section 3. The details of the FE simulations are described in Table 4.

The normal and shear stress levels of the aluminum slotted rod are predicted in two ways: prediction with the traditional method (assuming the Young's modulus of the Nylon is 12.25 GN/m^2, the average of E_x and E_y), and with our new similarity method:

(1) With the traditional method, the stress level of the aluminum rod can be approximately predicted from the following equation.

$$\mathbf{X}_T{}^A = \frac{E_{aluminum}}{0.5\cdot\left\{(E_x)_{nylon} + (E_y)_{nylon}\right\}}\cdot \mathbf{X}_P{}^A = 5.67\cdot \mathbf{X}_P{}^A \quad (42)$$

[2] The ratio of the Young's modulus in the x and y directions is exaggerated to illustrate the capability of the new similarity method.

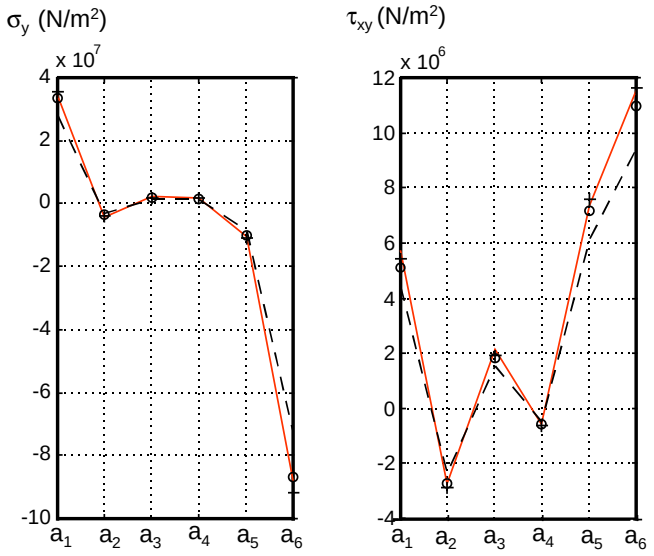

(a) y-directional normal stress (b) Shear Stress

Solid line: Actual (simulated) stress
Dotted line: Stress predicted with the approximate traditional similarity method (using the mean Young's modulus)
o : Stress predicted with the new empirical similarity method (using the measurements at the point set *A* of the specimen)
+ : Stress predicted with the new empirical similarity method (using the measurements at the point set *B* of the specimen)

Figure 6. Stress of the Slotted Rod at the Point Set *A*

where $\mathbf{X}_T^{\ A}$ and $\mathbf{X}_p^{\ A}$ are normal (or shear) stress vectors of the aluminum and nylon slotted rod at the point set *A*.
(2) With the new similarity method, the stress level of the aluminum rod is predicted from

$$\mathbf{X}_T^{\ A} = \mathbf{X}_P^{\ A} \cdot (\mathbf{X}_{PS}^{\ A})^{+} \cdot \mathbf{X}_{TS}^{\ A}, \text{ or}$$
$$\mathbf{X}_T^{\ A} = \mathbf{X}_P^{\ A} \cdot (\mathbf{X}_{PS}^{\ B})^{+} \cdot \mathbf{X}_{TS}^{\ B} \qquad (43)$$

where $\mathbf{X}_{TS}^{\ A}$, $\mathbf{X}_{PS}^{\ A}$ are stress vectors of the aluminum and the nylon specimen at the point set *A*, and $\mathbf{X}_{TS}^{\ B}$, $\mathbf{X}_{PS}^{\ B}$ are stress vectors at *B*. Both cases are examined to test the influence of the measuring points on the specimen, as mentioned earlier in this subsection.

The simulated normal and shear stress levels of the aluminum slotted rod and the stress predicted with the approximate traditional and new empirical similarity method are compared in Figure 6. The stress prediction with the approximated traditional method, shows non-negligible prediction error (error range: 7~32%, error mean: 18%), especially at a_1 and a_6. In comparison, the stress predicted with our new empirical similarity method shows good agreement (error range: 0.5~12%, error mean: 4%) with that of the ANSYS™ simulated aluminum slot. Although not shown due to space limitations, the prediction of the stress at the point set *B* also shows similar results.

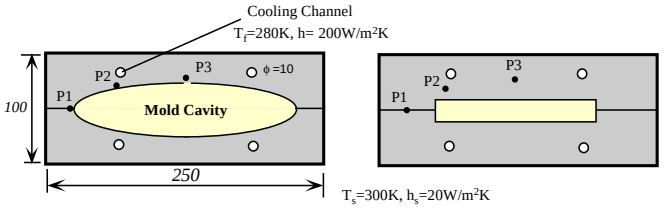

(a) Target Mold (b) Specimen Mold
Subscript s for exterior surface, f for cooling fluid (unit=mm)

Figure 7. Geometry and Boundary Conditions of Mold Dies

One interesting result to notice is the effect of the measurement points on the specimen. Even though the prediction error is increased at a_6, the stress prediction at the set *A* still shows good agreement when the stress vector at point set *B* is utilized instead of the stress vector at the set *A* (error range: 2~14%, error mean: 6%). So, one may choose a measurement point set without restrictions. Moreover, this interesting result may provide a way to quantify the prediction error bound, and/or to improve the prediction accuracy. One can refer to other numerical and experimental examples of static structural problems (e.g., correlation between two systems with small and large deflections, linear and nonlinear Young's modulus) in (Cho and Wood, 1997) for further examples.

4.2 Mold Design Example

Thermal modeling of molding processes is important to assure the quality of molded parts and to reduce molding cycle time. If the transient temperature distribution is not properly controlled, unwanted warpage or residual stress that lowers the product quality may be encountered. Some of the methods to control the temperature distribution are to adjust the geometric parameters of the mold die, to change the die material, and to include cooling channels. Among them, the inclusion of cooling channels can also increase productivity by reducing the molding cycle time (Sachs et al, 1995).

The objective of this example is to predict the transient temperature of an aluminum mold at points P1, P2, and P3 (Figure 7), during the solidification of melted tin. It is assumed that no reliable and cost effective rapid prototyping process is at hand that can fabricate aluminum molds. The geometry and boundary conditions of the target and specimen molds are shown in Figure 7a and 7b respectively. The boundary conditions of the aluminum and nylon molds are identical, excluding the cavity surfaces. The initial temperatures of the mold dies and filling materials are set to be identical and uniform. The initial temperature of the aluminum mold with melted tin is set to 550K, and that of the nylon molds with melted rubber is set to 375K. In Table 5, the material properties of the parts to be molded from the dies are listed, including

latent heat and enthalpy for modeling the solidification process. One can easily verify that the aluminum and nylon mold systems are highly distorted mainly due to material parameters and initial conditions. In this example, the transient temperature is predicted though two distinct empirical similarity methods: (1) the basic empirical similarity method that was introduced in subsection 3.3 (see Eq. 20); and (2) the modified empirical similarity method that is based on bilinear conformal mapping (Wylie and Barrett, 1982) in order to transform dependent and independent variables simultaneously. The details of the two methods are different, but the main concept is identical – utilization of the specimen to abstract the state transformation.

Unlike static problems, the transformation of both dependent (e.g., temperature) and independent (e.g., time) variables should be performed to solve transient or dynamic similarity problems. In order to maintain the dimension of the corresponding state vectors, the data is collected at $i \cdot t_f / N$, where $i=1,2,\ldots,N$, t_f is the measurement time span, and N is the dimension of the state vectors. In this example, the temperatures at P1, P2, and P3 are stored every 50 and 200 seconds (the time scale factor is set to 4, considering the thermal time constants $\tau=\rho VC_p/hA$ of aluminum and nylon) for the aluminum and nylon molds, respectively. The underlying assumption in this approach is that the time dependent system parameters do not significantly vary. Using Eq. 20, the temperature history at each point is predicted independently. According to Figure 8, the temperature history at P1 shows good agreement (it is similar for P2). However, the prediction error of the temperature history at P3 is not negligible. Some of the possible sources of error are simulation error caused by approximating smooth temperature-enthalpy curves with straight lines, inconsistency of time dependent parameters, and inadequacy of the linear state transformation.

In order to mitigate the prediction error, it is natural to consider a transformation that can transform both the time and temperature variables. As an initial approach, a bilinear transformation is constructed using the specimen pair as follows:

(1) Define complex variables z and w as

$$z_i = t_i^{PS} + T_i^{PS} j$$
$$w_i = t_i^{TS} + T_i^{TS} j \qquad (44)$$

where t_i and T_i denote the time and temperature at i-th discreterized temporal point, and the superscript PS and TS denote the prototype and target specimen respectively.

(2) By considering three distinct temporal points, one can derive the bilinear transformation $w = \frac{\alpha z + \beta}{\gamma z + \delta}$ (Wylie and Barrett, 1982)

(3) Approximate the temperature history of the nylon mold specimen at a spatial point, T(t) as a polynomial function.

(4) Using the polynomial T(t) of the nylon mold and the derived bilinear transformation, one can compute the temperature of the aluminum mold at the point.

As shown in Figure 8, the temperature history predicted with the modified empirical similarity method using the bilinear transformation shows remarkable agreement with the actual history, considering that the two systems are so highly distorted that even qualitative assessment is difficult (e.g., the point that shows the slowest temperature decrement is P2 in nylon molds, and P3 in aluminum molds).

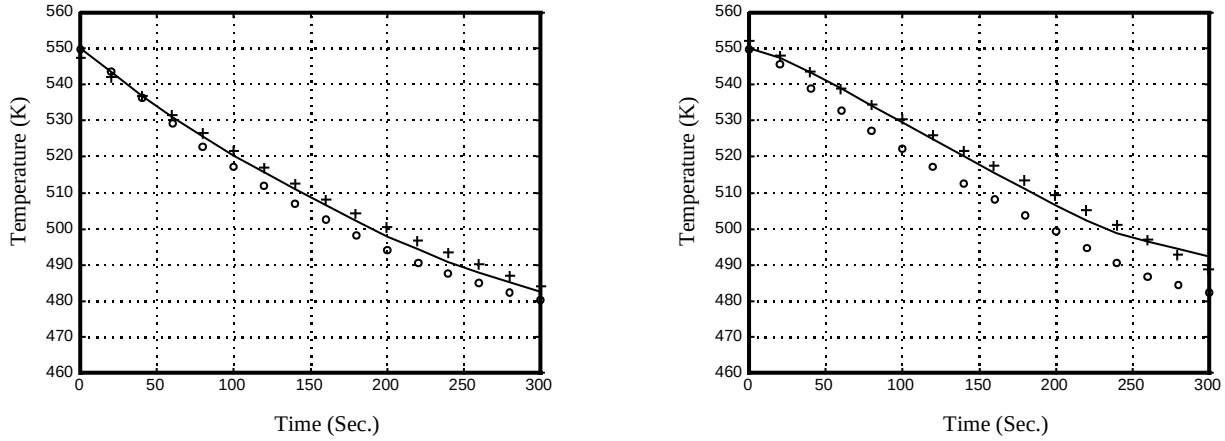

(a) Temperature at P1

(b) Temperature at P2

Solid line: Actual (simulated) temperature history
o : Temperature predicted with the new empirical similarity method (Pseudoinversion)
+: Temperature predicted with the modified empirical similarity method (Bilinear Conformal Mapping)

Figure 8. Transient Temperature of the Aluminum Mold

Table 5. Material Properties of Cavity Fillings

Material Properties	Tin	Rubber
Latent Heat (J/kg)	16,000	40,000
Melting Temperature (K)	505	370
Enthalpy (10^9 J/ m^3)	720 at T=450K 720.8 at T=500K 721.05 at T=500K	693 at T=330K 693.8 at T=350K 693.96 at T=370K
Thermal Conductivity k (W/m K)	66.6	0.13
Heat Capacitance C_p (J/kg K)	227	2010
Density ρ (kg/m^2)	7,310	1,100

In summary, the successful correlation of the thermal behavior of metallic and rapid prototyping molds can result in improved mold design providing high quality molds with reduced development cost and time. This is because the geometric complexity of mold cavities requires tremendous effort to fabricate physical models. Our method reduces the number of such models required. Also, the accuracy of virtual models is suspect; our method is based on physical measurements and is not subject to the same assumptions that are inherent in virtual models. Mold designers need tools that can cope with frequent introduction of new materials; our method provides a tool that generates reliable information for redesign. The extra prototyping effort required by our method is justified, since the extra prototypes are simpler geometrically, and even smaller improvements in mold quality are multiplied by the large production runs of molded parts.

5 DISCUSSION AND CONCLUSIONS

The new similarity method is developed to predict the functional behavior of geometrically complex products using rapid prototypes, when well-scaled physical modeling is difficult. In addition to the capability to solve distorted similarity problems, our method has several advantages over the traditional method: (1) Material properties need not to be known; (2) The effort to determine and control boundary conditions can be eliminated; and (3) One need not worry about potential error sources (e.g., negligence of dominant system parameters, identity of the configuration of governing equations).

In order to complete the new similarity method, two significant research issues must be addressed: (1) improvement of the prediction accuracy, and (2) development of a measure that can estimate the prediction error bound. Studies on improved state transformations, the effect of the measured state size, the influence of measurement error, and a strategy to improve the transformation when more than one specimen pair is available, are some of the approaches to improve the novel empirical similarity method. Plausible alternative state transformation methods include linear transformation including higher order terms, and analytical polynomial transformation including independent variables. Parallel to the effort to improve the prediction accuracy, an error measure should be provided so that designers can make informed decisions. Neither the traditional nor our new method can be verified until multiple tests are performed. However, the new method may provide insights from test results, by considering two routes that transform the states of the prototype specimen and the target, one through the prototype and the other through the product specimen. The transformations of the two routes should be identical if the prediction is perfect. Thus a relationship between these two transformations may be treated as an error measure.

ACKNOWLEDGMENT

The research reported in this document was made possible, in part, by a Young Investigator Award from the National Science Foundation. The authors also wish to acknowledge the support of Ford Motor Company Texas Instruments, Desktop Manufacturing Corporation, and the UT June and Gene Gills Endowed Faculty Fellow. Any opinions, findings, or recommendations are those of authors and doe not necessarily reflect the views of the sponsors.

REFERENCES

Aubin, R.F., "A World Wide Assessment of Rapid Prototyping Technologies," Proceedings of Solid Freeform Fabrication Symposium Proceedings, Austin TX, August, 1994, pp.118-145.

Baker, W.E. and Westine, P.S., "Model Tests for Structural Response of Apollo Command Module to Water Impact," Journal of Spacecraft, 4(2), February 1967, pp.201-208.

Baker, W.E., Westine, P.S., Dodge, F.T., Similarity Methods and Engineering Dynamics: Theory and Practice of Scale Modeling, Elsvier, 1991.

Barr, D., "Consolidation of Basics of Dimensional Analysis," Journal of Engineering Mechanics, ASCE, 10(9), September, 1984, pp. 1357-1375.

Bazant, Z.P., "Scaling Laws in Mechanics of Failure," Journal of Engineering Mechanics, ASCE, 119(9), September, 1993, pp. 1828-1844.

Beck, J.E. et al, "Manufacturing Mechatronics using Thermal Spray Shape Deposition," Proceedings of Solid Freeform Fabrication Symposium, Austin TX, August, 1992, pp.272-279.

Birley, A.W., Heath, R.J., and Scott, M.J., *Plastics Materials: Properties and Applications*, Blackie & Son Ltd., New York, 1988.

Bluman, G.W., Kumei, S., *Symmetries and Differential Equations*, Springer-Verlag, New York, 1989.

Burton, R.A. and Carper, H.J., "An Experimental Study of Annular Flow with Applications to Turbulence Film Lubrication," ASME Journal of Lubrication Technology, Vol.39, 1967, pp. 381-391.

Cho, U. and Wood, K.L., "Empirical Similitude Method for the Functional Test with Rapid Prototypes," Proceedings of Solid Freeform Fabrication Symposium, Austin TX, September, 1997, pp.559-567.

Das, S. et al., “Direct Selective Laser Sintering and Containerless Hot Isostatic Pressing for High Performance Metal Components,” Proceedings of Solid Freeform Fabrication Symposium, Austin TX, September, 1997, pp.81-90.

Dornfield W.H., “Direct Dynamic Testing of Scaled Stereolithographic Models,” Sound and Vibration, August 1995, pp. 12-17.

Elliott, W., “Plastic Models for Structural Analysis,” U S Naval Research Lab., Shock and Vibration Bulletin n40 pt 4, Dec. 1969, pp. 89-96.

El-Zafrany, A., *Techniques of the Boundary Element Method*, Ellis Horwood Ltd., 1993.

Erhun, M. and Advani, S.G., “Heat Transfer Effects during Solidification of Semicrystalline Polymers,” ASME Journal of Engineering Materials and Technology, Vol. 115, January, 1993, pp. 30-36.

Farrar, C.R., Baker, W.E., and Dove, R.C., “Dynamic Parameter Similitude for Concrete Models,” ACI Structural Journal, V. 91, No. 1, 1994, pp.90-99.

Fay, R.J., “Scale Model Tests of Vehicle Motions,” Vehicle and Occupant Kinematics: Simulation and Modeling SAE Special Publication n 975, SAE, pp51-54, 1993.

Fertis, D.G., *Nonlinear Mechanics*, CRC Press, Inc., 1993.

Fessler, J.R. et al., “Functional Gradient Metallic Prototypes through Shape Deposition Manufacturing,” Proceedings of Solid Freeform Fabrication Symposium, Austin TX, September, 1997, pp.521-528.

Gipson, G.S., *Boundary Element Fundamentals - Basic Concepts and Recent Developments in the Poisson Equation*, Computational Mechanics Publications, 1987.

Griffith, M.L. et al. (1997) Multiple-Material Processing by LENS, Proceedings of Solid Freeform Fabrication Symposium, pp.387-394.

Halwel, D., Klameckl, B.E., “Characterization of Force Sensors Embedded in Surfaces for Manufacturing Process Monitoring,” ASME Manufacturing Science and Engineering, Vol.64, pp.207-216.

Ingham, D.B. and Yuan, Y., *The Boundary Element Method for Solving Improperly Posed Problems*, Computational Mechanics Publications, 1994.

Jacobs, P. F., *Rapid Prototyping and Manufacturing: Fundamentals of StereoLithography*, Society of Manufacturing Engineers, McGraw-Hill Inc., 1992.

Jepson, L. et al, “SLS processing of Functionally Gradient Materials,” Proceedings of Solid Freeform Fabrication Symposium, Austin TX, September, 1997, pp.67-80.

Kline, S.J., *Similitude and Approximation Theory*, McGraw-Hill Co., New York, 1965.

Mixon, J.S. and Catherine, J.J., “Comparison of Experimental Vibration Characteristics for a 1/5-Scale Model and from a Full-Scale Saturn AS-1,” TN D-2215, NASA, 1964.

Murphy, G. (1971) “Models with Incomplete Correspondence with the Prototype,” Journal of the Franklin Institute, 292(6), pp.513-518.

Nelson J.C., et al, “Post-Processing of Selective Laser Sintered Polycarbonate Parts,” Proceedings of Solid Freeform Fabrication Symposium, Austin TX, August, 1993, pp. 78-85.

Prinz, M.R., “Shape Deposition Manufacturing,” Proceedings of Solid Freeform Fabrication Symposium, Austin TX, August, 1994, pp. 1-8.

Sachs, E. et al., “Production of Injection Molding Tooling with Conformal Cooling Channels using the Three Dimensional Printing Process,” Proceedings of Solid Freeform Fabrication Symposium, Austin TX, August, 1995, pp. 448-467.

Safari, S. et al, “Processing of Novel Piezoelectric Transducers Via SFF,” Proceedings of Solid Freeform Fabrication Symposium, Austin TX, September, 1997, pp.403-410.

Smith, S.H. et al. (1992) “A Calibration Approach for Smart Structures Using Embedded Sensors,” Experimental Techniques, March/April, pp.25-31.

Steinchen, W., Kramer, B., Kupfer, G., “Photoelastic Investigation Using New STL-Resins,” Proceedings of Solid Freeform Fabrication Symposium, Austin TX, August, 1995, pp.204-212.

Strang, G, *Linear Algebra and Its Applications*, Harcourt Brace Jovanovich, Inc., 1988.

Sun, L. et al, “Fabrication of In-situ SiC/C Thermocouples by SALD,” Proceedings of Solid Freeform Fabrication Symposium, Austin TX, September, 1997, pp.481-488.

Wall, M.B. et al., “Making Sense of Prototyping Technologies for Product Design,” ASME 3rd International Conference on Design Theory and Methodology, Vol.31, 1991, pp. 157-164.

Wright, D.V., and Bannister, R.C., “Plastic Models for Structural Analysis – Part 1: Testing Types,” The Shock and Vibration, 2, 11, 1971, pp. 2-10.

Wylie, C.R. and Barrett, L.C., *Advanced Engineering Mathematics*, McGraw-Hill, Inc., New York, 1982.

APPENDIX

1 Derivation of the State at the Interface

As the interface state of the prototype specimen, $\phi_I{}^p$, should satisfy Eq. (27),

$$\begin{aligned}&(r_{41}{}^{p1} + r_{42}{}^{p1} + r_{43}{}^{p1}) \cdot \phi_a + r_{44}{}^{p1} \cdot \phi_I{}^p \\ &= -(r_{21}{}^{p2} + r_{23}{}^{p2} + r_{24}{}^{p2}) \cdot \phi_b - r_{22}{}^{p2} \cdot \phi_I{}^p .\end{aligned} \tag{A.1.1}$$

From Eq. (A.1.1),

$$\begin{aligned}\phi_I{}^p &= \frac{-1}{r_{44}{}^{p1} + r_{22}{}^{p1}} \cdot \left\{ \begin{matrix} (r_{41}{}^{p1} + r_{42}{}^{p1} + r_{43}{}^{p1}) \cdot \phi_a \\ + (r_{21}{}^{p2} + r_{23}{}^{p2} + r_{24}{}^{p2}) \cdot \phi_b \end{matrix} \right\} \\ &= C(r_{44}{}^{p1} + r_{22}{}^{p1}) \cdot \left[\phi_a \cdot f_a(\mathbf{r}_4{}^{p1}) + \phi_b \cdot f_b(\mathbf{r}_2{}^{p2}) \right].\end{aligned} \tag{A.1.2}$$

Similarly, the interface state of the target specimen, $\phi_I{}^t$ becomes

$$\phi_I{}^t = \frac{-\left\{(r_{41}{}^{t1} + r_{42}{}^{t1} + r_{43}{}^{t1}) \cdot \phi_a + (r_{21}{}^{t2} + r_{23}{}^{t2} + r_{24}{}^{t2}) \cdot \phi_b\right\}}{r_{44}{}^{t1} + r_{22}{}^{t1}}$$

$$= C(r_{44}{}^{t1} + r_{22}{}^{t1}) \cdot \left[\phi_a \cdot f_a(\mathbf{r}_4{}^{t1}) + \phi_b \cdot f_b(\mathbf{r}_2{}^{t2})\right]. \qquad \text{(A.1.3)}$$